Photofission of ^{232}Th and ^{238}U at intermediate energies

A. Deppman,[1] E. Andrade-II,[1] V. Guimarães,[1] G. S. Karapetyan,[1] and N. A. Demekhina[2]
[1]*Instituto de Fisica, Universidade de Sao Paulo Travessa R da Rua do Matao, 187, 05508-900 Sao Paulo, SP, Brazil*
[2]*Yerevan Physics Institute, Alikhanyan Brothers 2, Yerevan 0036, Armenia Joint Institute for Nuclear Research (JINR), Flerov Laboratory of Nuclear Reactions (LNR), Joliot-Curie 6, Dubna 141980, Moscow region Russia*
(Received 14 December 2012; revised manuscript received 26 February 2013; published 6 May 2013)

In this work we present an analysis of the yields of fission fragments induced by bremsstrahlung photons with endpoint energies of 50 and 3500 MeV on ^{232}Th and ^{238}U targets using the simulation code CRISP. A multimodal fission option was added to this code and an extension of the calculation to the properties of the fission products is presented. By dividing the fissioning nuclei according to their fissionability, an approach is introduced which accounts for the contribution of symmetric and asymmetric fission. By adopting this procedure, it was possible to calculate the main parameters for the fission-fragment charge distribution such as the most-probable charge for a given fission product mass chain and its corresponding width parameter. Also, it was possible to reproduce features of fragment mass distribution and evaluate the fissility of fissioning nuclei for photon-induced fission of ^{232}Th and ^{238}U.

DOI: 10.1103/PhysRevC.87.054604 PACS number(s): 25.85.Jg

I. INTRODUCTION

Despite almost seventy years of investigations on nuclear fission, this process still continues to be of great interest. The disintegration of the nucleus into two fragments of similar masses is accompanied by a complete rearrangement of the nuclear structure, and the dynamical process leading to fission determines the characteristics of the fragments in the final states. Investigation of the photofission process in heavy nuclei is very interesting not only for the study of the fission mechanism itself, but also to obtain information about total photoabsorption [1–3]. Photons provide a convenient tool to study nuclear properties of a fissile system and to explore nuclear transformations at large deformations. In the case of photonuclear reactions, volume absorption dominates and, as a result, the photon effectively "heats" the nucleus. For this reason, the excitation of the nucleus in different energy ranges reflects the nature of the interaction with incident photons. In the analysis of experiments with bremsstrahlung photons, the calculations of the total photofission yield takes into account the contributions of the different interaction modes by summing over the entire spectrum of photons.

The calculation of fission cross section within different models and their comparison with data provides an opportunity to estimate the validity of the various photoabsorption mechanisms as well as to investigate characteristics of the processes taking place in reactions induced by different probes. Among the properties that can be used to compare calculations with data are charge and mass distributions of the fragments, energy dependence of the fission cross section, and the ratio of symmetric and asymmetric components of fission products. In the present work, calculations for fragments produced in photofission of heavy nuclei, ^{232}Th and ^{238}U, induced by bremsstrahlung photons with endpoint energies of 50 and 3500 MeV are presented. The most important quantities calculated are mass and charge distributions for each of the target nuclei at the two energies of 50 and 3500 MeV. Comparison with data is performed and the analysis allows the extraction of information about the fission process following the absorption of the photon. The data considered here were obtained from experiments described in detail elsewhere [4,5] and the calculations were performed with the CRISP code [6].

II. CRISP CODE

CRISP is a Monte Carlo code which simulates, in a two-step process, nuclear reactions induced by photons or protons [6]. First, an intranuclear cascade is simulated following a time-ordered sequence of collisions in a many-body system [7,8] and, when the intranuclear cascade finishes, the evaporation of nucleons and alpha particles begins, in competition with the fission process [9]. In the simulation, reactions can be initiated by intermediate- and high-energy protons [8] or photons [10–12]. The CRISP code has been shown to be reliable in reproducing photon-induced reactions and gave good results for total photonuclear absorption cross sections for energies from approximately 50 MeV, where the quasideuteron absorption mechanism is dominant, up to 3.5 GeV, where the so-called photon-hadronization mechanism leads to a shadowing effect in the cross section [13].

One important feature of the code, in simulating the intranuclear cascade, is the Pauli blocking mechanism, which avoids violation of the Pauli principle. In the CRISP code a strict verification of this principle is performed at each step of the cascade, resulting in a more realistic simulation of the process. The advantages of such an approach have been discussed elsewhere (see, for instance, Ref. [6] and references therein). In the evaporation-fission competition that follows the intranuclear cascade, Weisskopf's model is adopted to calculate the branching ratios of the evaporating channels, which includes evaporation of neutrons, protons, and alpha particles [9,11,12], and the Bohr-Wheeler model is adopted for fission. When one particle is emitted during the evaporation process, the excitation energy of the final-state nucleus is calculated by $E_x^{(f)} = E_x^{(i)} - (B + V + \varepsilon)$, where $E_x^{(f)}$ and $E_x^{(i)}$ are the excitation energy of the final and initial nucleus, respectively, B is the evaporated particle separation energy,

V is its Coulomb potential, and ε is the mean kinetic energy of the emitted particle, which is fixed at 2 MeV. The code has provided good agreement of photofission cross-section data [6]. The CRISP code has also already been used to evaluate mass distributions of fragments for fission induced by photons at intermediate energies [14] and to calculate spallation yields and neutron multiplicities for reactions induced by high-energy protons [15], giving results in good agreement with data. Moreover, the code has already been used in studies of the Accelerator Driving System (ADS) nuclear reactors [15–18].

III. DESCRIPTION OF MODEL AND CALCULATIONS

The fission process has been successfully described by the multimodal random neck rupture model (MM-RNRM) [19], which takes into account the collective effects of nuclear deformation during fission through a liquid-drop model and includes single-particle effects through microscopic shell-model corrections. The microscopic corrections create valleys in the space of elongation and mass number, each valley corresponding to a different fission mode [19]. In the MM-RNRM, the yield of fragments is described for each mode by a Gaussian distribution which is characterized by the fragment's mass and atomic numbers A and Z, respectively. According to this model, the mass-yield curve can be decomposed into three distinct fission components: one symmetric Superlong and two asymmetric, Standard I and Standard II. Superlong-mode fragments are strongly elongated with masses around $A_f/2$. The Standard I mode is characterized by the influence of the spherical neutron shell $N_H \sim 82$ and proton shell $Z_H \sim 50$ in the heavy fragments with masses $M_H \sim 132$–134. The Standard II mode is characterized by the influence of the deformed neutron shell closure $N = 86$–88 and proton shell $Z_H \sim 52$ in the heavy fragments with masses $M_H \sim 138$–140. There is a new investigation of the influence of shell closures by Schmidt and Jurado [20] indicating that the fission of a large number of isotopes is governed not by the neutron closed or deformed shells at $N = 82$ or $N = 88$ but by the proton number $Z = 54$. Here we consider that fission can take place through one of these three different modes, and that the total mass yield is obtained by the sum of the three Gaussian functions [21]:

$$Y_A = \frac{1}{\sqrt{2\pi}}\left[\frac{K_{1AS}}{\sigma_{1AS}}\exp\left(-\frac{(A-A_S-D_{1AS})^2}{2\sigma_{1AS}^2}\right)+\frac{K'_{1AS}}{\sigma'_{1AS}}\exp\left(-\frac{(A-A_S+D_{1AS})^2}{2\sigma_{1AS}'^2}\right)+\frac{K_{2AS}}{\sigma_{2AS}}\exp\left(-\frac{(A-A_S-D_{2AS})^2}{2\sigma_{2AS}^2}\right)\right.$$
$$\left.+\frac{K'_{2AS}}{\sigma'_{2AS}}\exp\left(-\frac{(A-A_S+D_{2AS})^2}{2\sigma_{2AS}'^2}\right)+\frac{K_S}{\sigma_S}\exp\left(-\frac{(A-A_S)^2}{2\sigma_S^2}\right)\right], \quad (1)$$

where A is the fragment mass number, A_S is the mean mass number which determines the center of the Gaussian functions, and K_i, σ_i, and D_i are the contribution, dispersion, and position parameters of the ith Gaussian functions. The indices AS and S designate the asymmetric and symmetric components. Note that, when using the CRISP code, it is possible to work on event-by-event basis, and therefore the parameter A_S in Eq. (1) is completely determined by the mass of the fissioning nucleus; that is, $A_S = A_{ff}/2$. During the calculation, we have defined two types of fissioning nuclei: before (A_f) and after (A_{ff}) postfission neutron evaporation, where $A_H + A_L = A_{ff}$, and the indices H and L stand for heavy- and light-mass fragments. The quantities $A_S + D_{iAS} = \mathrm{A}_H$ and $A_S - D_{iAS} = \mathrm{A}_L$ determine the positions of the heavy and light peaks of the asymmetric components on the mass scale. The values of $A_H + A_L$ and $2A_S$ were treated as the masses of nuclei that undergo fission in the respective channel. Typical values for these parameters obtained in a fitting process can be found in Refs. [4,5].

The fragment charge distribution can be estimated by considering the Gaussian functions in the form [22,23]

$$Y_{A,Z} = \frac{Y_A}{\Gamma_z \pi^{1/2}}\exp\left(-\frac{(Z-Z_p)^2}{\Gamma_z^2}\right), \quad (2)$$

where $Y_{A,Z}$ is the independent yield of the nuclide (Z, A), Y_A is the total yield for a given mass number A, Z_p is the most-probable charge for isobars with mass number A, and Γ_z is the width parameter. The parameters Z_p and Γ_z can be represented as slowly varying linear functions of the mass numbers of fission fragments:

$$Z_p = \mu_1 + \mu_2 A\,, \quad (3)$$

and

$$\Gamma_z = \gamma_1 + \gamma_2 A\,. \quad (4)$$

The multimodal model has been used previously to describe spontaneous fission [24], low-energy induced fission [25], fission induced by thermal neutrons [26–28] and 12 MeV protons [29], and even fission induced by intermediate-energy probes such as 190 MeV protons [23], neutrons at energies up to 200 MeV [30], and also by heavy ions [31,32].

The CRISP code was then adapted to consider the multimodal model by the use of Eqs. (1) and (2). To determine the fission-fragment masses by the CRISP code it is necessary to attribute values for the parameters used in the multimode approach, which is not a trivial problem. Since the CRISP code simulates the entire process up to the point of fission, the fissioning nucleus of all events is known, which leads to the fact that A_S cannot be taken as a free parameter but as a distribution instead. Therefore, at every point of decision on the fission channel, the appropriate value for A_S is used considering the nucleus which is undergoing fission. Whenever the fission channel is chosen, the masses and atomic numbers of the heavy fragments produced, A_H and Z_H, respectively, are sorted according to

Eq. (1). The light fragments are obtained according to $A_L = A_f - A_H$ and $Z_L = Z_f - Z_H$, where A_f and Z_f are the mass and atomic number of the fissioning nucleus, respectively. As mentioned, A_S is the average mass number of the fragments for the symmetric component, which determines the center of the Gaussian function. It is related to the mass of the fissioning nucleus by $2A_S = A_f$, where $A_f = A_H + A_L$.

As a final step, all fragments obtained in the above fashion evaporate according to the model of evaporation-fission competition already mentioned. The energy of each fragment is determined using

$$E_i = \frac{A_i}{A_f} E_{\text{frag}}, \tag{5}$$

where E_i and A_i are the excitation energy and the mass number of the fragment i. E_{frag} is the total excitation energy of the fragments which is assumed, as an approximation, to be equal to the excitation energy of the fissioning system.

IV. RESULTS AND DISCUSSION

The CRISP code is used here to analyze data on fission-fragment distributions produced by photofission of ^{232}Th and ^{238}U. The data were obtained from radiation of bremsstrahlung photons on ^{232}Th and ^{238}U targets. The bremsstrahlung photons with endpoint energies of 3500 and 50 MeV were obtained with the Yerevan electron synchrotron and a linear accelerator of injector type, respectively. In these measurements, the electrons were converted into a bremsstrahlung photon beam by means of a tungsten converter of about 300 μm. The photon-beam intensity was determined with a Wilson-type quantameter, and the obtained average values were 10^{11} and 10^9 equivalent photons per second at the maximum energy of 3500 MeV and 50 MeV, respectively. The ^{232}Th and ^{238}U targets were 20 and 70 μm thick, respectively. The yields of radioactive fission fragments were measured in offline mode with a HpGe semiconductor detector. The energies of the gamma transitions and the relations between their intensities, as well as half-lives, were used to select reaction products and to determine their yields. Measurements of the gamma spectra started about 120 minutes after the irradiation was finished and lasted for a year. More details on these experiments can be found in Refs. [4] and [5].

Usually, in such offline analyses, the detected fragments represent the final products of the fission process after neutrons and gamma rays are emitted from both the fissioning nucleus and the primary fragments. Thus, comparison between calculation and experiment allows the unfolding of the contributions of pre- and postscission neutron emissions. Here we are considering the charge and mass characteristics of the fission products to obtain information about the hot nuclear system and its decay channels.

A. Charge distribution

As discussed above, according to Eq. (2), the charge distribution for an isobar chain with mass number A, from a fissioning heavy nucleus, is characterized by a Gaussian shape with parameters Z_p and Γ_z, where Z_p and Γ_z are the most-probable charge and the corresponding width of the distribution. The best representation regarding the most-probable charge Z_p is a linear function of the mass of the fission fragment, as given by the empirical Eq. (3) [33]. Although these parameters have a linear dependence on A, through Eqs. (3) and (4), respectively, the Γ_z are experimentally determined to be practically independent of A [22,33,34].

In Table I, we summarized the experimental and calculated relevant parameters μ_1, μ_2, γ_1, and γ_1 used in the present work to determine Z_p and Γ_z. As one can see, the calculated parameter γ_2 is very small for all four cases, indicating that Γ_z is almost constant. Experimentally, instead of considering the Γ_z, we averaged the full width at half maximum (FWHM) of all charge distributions. The small deviation around the average values is another indication that this parameter is practically independent of A. Although it has been experimentally observed that the width of charge distribution Γ_z is independent of A, there is a small mass dependence in the calculated values given by the parameter γ_2 in Eq. (3) and shown in Table I. From the value of the FWHM and γ_2 in Table I, it is clear that, as the excitation energy increases, the charge distribution becomes slightly wider. In general, a similar dependence was observed in fission induced by particles of different types at excitation energies up to 100 MeV [35].

In Fig. 1 we plot the difference between the calculated and experimental values for Γ_z of the charge distributions for the ^{238}U and ^{232}Th targets at the two endpoint energies. It is possible to observe that the overall difference is around ± 0.3 units, corresponding to approximately 25% of the total width Γ_z, and that the difference is in the same range for both endpoint energies. The deviation between calculation and experiment presents an approximately linear increase with

TABLE I. Parameters used to determine experimental and calculated charge distributions.

Parameter	^{238}U		^{232}Th	
	$E_{\text{max}} = 50$ MeV	$E_{\text{max}} = 3500$ MeV	$E_{\text{max}} = 50$ MeV	$E_{\text{max}} = 3500$ MeV
$(\mu_1)_{\text{expt}}$	5.70 ± 0.60	5.32 ± 0.62	3.89 ± 0.67	4.14 ± 0.70
$(\mu_2)_{\text{expt}}$	0.356 ± 0.005	0.362 ± 0.005	0.371 ± 0.005	0.356 ± 0.005
$(\mu_1)_{\text{calc}}$	4.10	4.10	5.00	5.00
$(\mu_2)_{\text{calc}}$	0.380	0.380	0.370	0.370
$(\gamma_1)_{\text{calc}}$	0.92	0.92	0.59	0.59
$(\gamma_2)_{\text{calc}}$	0.003	0.003	0.005	0.005
FWHM	1.03 ± 0.12	1.09 ± 0.13	1.13 ± 0.14	1.14 ± 0.15

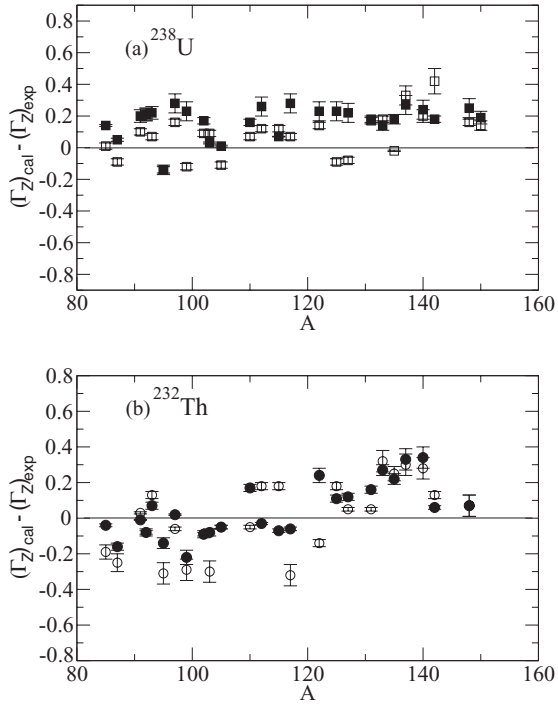

FIG. 1. Difference between experimental and calculated values by the CRISP code for the width of the charge distribution for (a) ^{238}U and (b) ^{232}Th targets. The open-square and open-circle symbols are for data taken at $E_{max} = 50$ MeV while the solid-square and solid-circle symbols were taken at $E_{max} = 3500$ MeV.

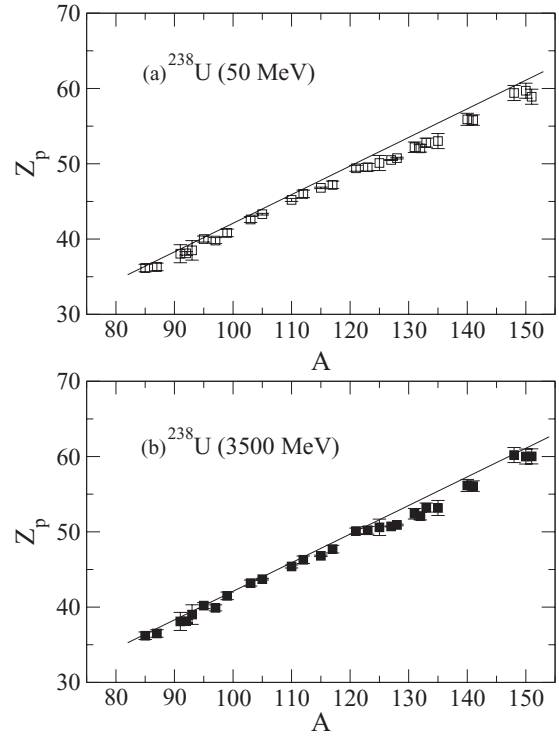

FIG. 2. Most-probable charge Z_p for induced photofission on ^{238}U target at bremsstrahlung photon endpoint energies of (a) 50 and (b) 3500 MeV. The black solid lines are the results of calculations by CRISP.

mass number A for all four cases studied, going from -0.3 for $A \approx 85$ to $+0.3$ for $A \approx 150$. The fluctuation observed in this deviation seems to be a manifestation of fragment shell effect ($Z_p \sim 50$), which might not have been completely taken into account by the linear parametrization of Eqs. (3) and (4). This effect can be clearly seen in the direct comparison of calculated and experimental most-probable charge Z_p shown in Figs. 2 and 3 for the ^{238}U and ^{232}Th targets, respectively. Figures 2 and 3 show both the experimental values of the most-probable charge Z_p and the values calculated by the CRISP model for ^{238}U and ^{232}Th, respectively, at the two incident energies. In general, the experimental values of Z_p cogently fit to those obtained by model calculations. To be more quantitative, the reduced χ^2 was used to evaluate the comparison between data and CRISP calculations. The results obtained are, for ^{238}U, $\chi^2 = 0.80$ at $E_{max} = 50$ MeV and $\chi^2 = 0.54$ for $E_{max} = 3500$ MeV; and for ^{232}Th: $\chi^2 = 0.66$ for $E_{max} = 50$ MeV; $\chi^2 = 0.38$ at $E_{max} = 3500$ MeV. It can be noticed that both calculated values and data present an overall linear trend with the mass number A, as given by the parameters μ_1 and μ_2.

As one can see in Table I, the values of the calculated parameters μ_2 for the uranium isotope, at both energies, are slightly higher than the experimental values. As a result, the values obtained for the most-probable charge Z_p for a given mass number are shifted to a larger value (more neutron deficient). In Figs. 2 and 3 one can see that the calculated values for Z_p are mostly on the left side (i.e., proton-rich side) of the experimental values, especially for low-energy fission for both isotopes. This is a reflection of the dependence of the parameter μ_2 on charge and mass of the fissioning nucleus and, thus, on the average number of emitted neutrons from the fission fragments [22]. The calculated values for the parameter μ_1 are about one unit below the experimental values for the uranium target at both energies and one unit above for the thorium target. The higher measured values for μ_1, in comparison with the calculated values, indicate that the calculation favors a most-probable charge for the fission products of uranium target closer to the stable nucleus. With the increase of excitation energy and the atomic number of the fissioning nucleus, one would expect that Z_p of an isobaric chain would become closer to the Z values of a more stable nucleus. Therefore, the model is considering greater evaporation of neutrons from the fission fragments. In the case of thorium the situation is the opposite, but the agreement with calculated values is better. We can assert that the model considers more correctly the evaporation of neutrons for the Th target. Also, as one can see in both Figs. 2 and 3, for A around 125, the data show a slight deviation between calculated and experimental Z_p values in the region of $A > 130$. This deviation is more prominent in the case of the ^{238}U target. These results suggest that the CRISP calculation can be improved by including shell effects in the parametrization of Z_p. However, aside from the slight deviation discussed above, the calculation seems to present a general small shift to neutron-deficient fragments, which also can be corrected in the next upgraded version of the code.

This analysis of parameter values shows that, in general, the CRISP model describes fairly well the most-probable charge

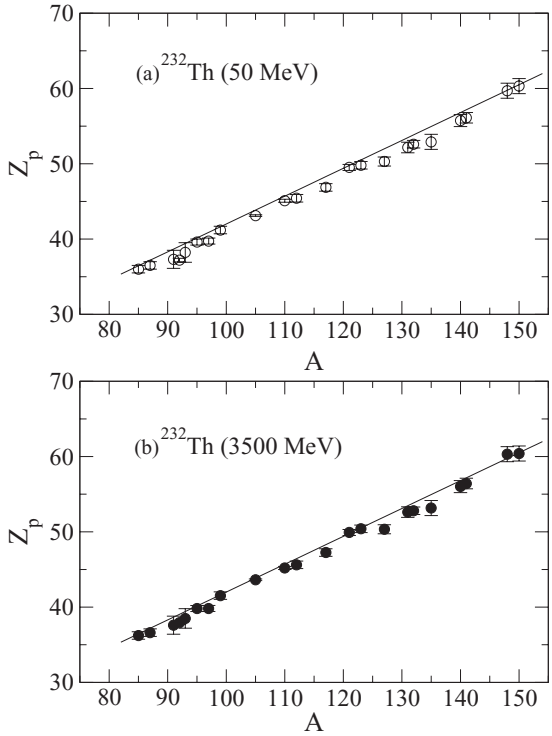

FIG. 3. Most-probable charge Z_p for induced photofission on ^{232}Th target at bremsstrahlung photon endpoint energies of (a) 50 and (b) 3500 MeV. The black solid lines are the results of calculations by CRISP.

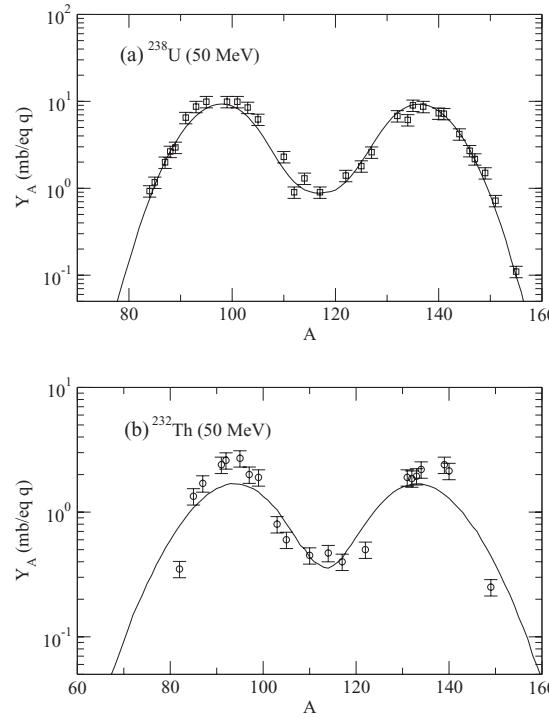

FIG. 4. Mass distribution, mass yield as a function of mass number in units of mb per equivalent quanta (mb/eq.q) at E_{max} = 50 MeV for (a) ^{238}U and (b) ^{232}Th targets. The solid line is the result of a CRISP calculation.

of the charge distribution for the fission fragments for ^{232}Th and for ^{238}U, with some fluctuations in Γ_z. It can, however, be assumed that the model takes into account the main properties of fissile systems and provides a way to predict some characteristics of the fragment charge distribution.

As can be observed in the data, as we increase the endpoint energy the composite system has a higher excitation energy producing, on average, fissioning nuclei with less neutrons due to the higher number of evaporated neutrons (proton evaporation is suppressed due to the Coulomb barrier). As a consequence, the following produced heavier fragments will also evaporate more neutrons and, as a result, the fragments with same A will have larger Z shifting, on average, the Z_p parameter to higher values. Similar behavior is observed for fission induced by different probes such protons and neutrons on ^{238}U and ^{232}Th [22,36–38], indicating that the charge distributions are determined more by the excitation energy and nuclear properties of the reaction products than by the choice of projectile.

B. Mass distribution

The origin of asymmetric fission is associated with the shell structure of the fissioning nucleus and nuclear fragments [39], whereas symmetric fission is consistent with a classical liquid-drop model of the fissioning nucleus [40], and it is the most relevant mechanism for fission of highly excited (>50 MeV) nuclei. Therefore, mass distributions of fragments depend on the mass of the fissioning nuclei and on its excitation energy.

The calculations with the CRISP code consider the three-mode hypothesis discussed previously, corresponding to one symmetric (Superlong) and two asymmetric dynamics (Standard I and Standard II). The results obtained allow a complete analysis of the fragment-mass distributions for ^{238}U and ^{232}Th. The total fission mass-yield distribution as a function of the product mass number (A) for ^{238}U and ^{232}Th targets at E_{max} = 50, 3500 MeV are shown in Figs. 4(a), 4(b), 5(a) and 5(b), respectively. Qualitatively, the agreement between the calculation and the experimental data is fairly good at both endpoint energies, particularly for low energies, where the calculations reproduce the experimental data quite well. This fact shows that the model correctly takes into account the influence of shell effects for low-energy fission, associated with asymmetric fission modes: the strong spherical neutron shell at N = 82 and the deformed neutron shell at N = 86–88 become dominant and lead to asymmetric fission. It is also possible to observe in Figs. 4 and 5 that a better agreement between calculation and data is achieved for the lower endpoint energy. This can be due to the fact that the parameters used in Eq. (1) are based on a systematic analysis for low-energy fission, which may not be as good for higher energies. To a lesser extent, by comparing the results for ^{232}Th with those for ^{238}U, one can observe that, for uranium, the agreement with data is better for both endpoint energies. This also can be due to the fact that the systematics used to set the parameters was done for $A > 220$, and the results extrapolated to lower mass. It is possible to conclude that the values for D and Γ for $A < 220$ are somewhat overestimated.

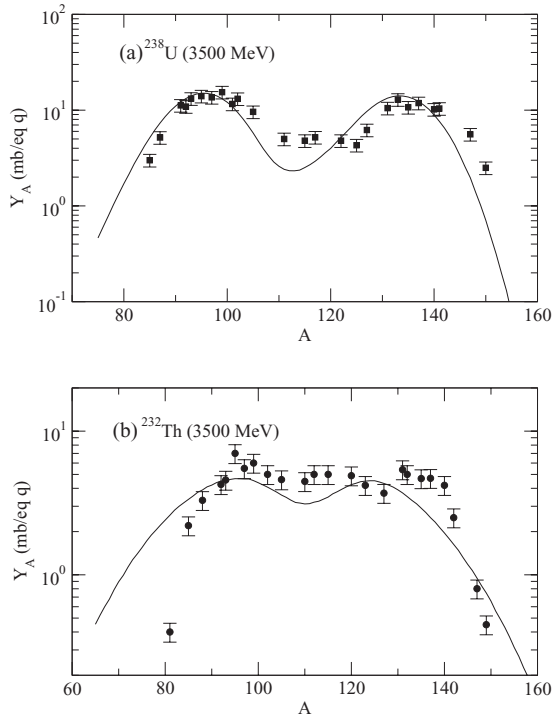

FIG. 5. Mass distribution, mass yield as a function of mass number in units of mb per equivalent quanta (mb/eq.q), at $E_{\max} =$ 3500 MeV for (a) ^{238}U and (b) ^{232}Th targets. The solid line is the result of a CRISP calculation.

Another parameter that can be used to compare data and calculations is the integrated total fission yield Y_F, given by

$$Y_F = \frac{1}{2}\int Y_A(A)dA. \quad (6)$$

The result of this calculation together with data on total fission yields in units of mb per equivalent quanta (mb/eq.q) as well as some other calculated quantities and their corresponding experimental values are listed in Table II for comparison.

At intermediate energies the discrepancy between experiment and calculation becomes larger for all observed parameters, except for total fission yield values. The reason for this can be due to the character of bremsstrahlung. As the latter has a continuous spectrum, the measurements at high energy include also low-energy photons. From the calculated mass distribution it can be concluded that the model underestimates the low-energy part of the bremsstrahlung spectrum. The calculated mean mass number of distributions after evaporation of postscission neutrons $(A_{ff})_{\text{calc}}$ is shifted to lower masses in comparison to the experimental ones with increasing energy. It means that the yields of symmetric fission fragments grow faster, because of the considerable amount of high-energy photons.

Moreover, we also calculated the mass-yield distribution of the fissioning nuclei, before they undergo fission, which are shown in Fig. 6. This figure allows the comparison of the fissioning system distributions for thorium and uranium targets at both endpoint energies. These distributions result from a complex balance between evaporation and fission processes. Apart from the obvious fact that there are no fissioning nuclei with mass $A > 232$ for the case of ^{232}Th, the fissioning-nucleus distribution extends much below the range of those systems in the case of ^{238}U. It is clear that low mass nucleus fragments are more abundant in the case of thorium fission distribution than in the case of uranium. One of the consequences of the predominance of low-mass nuclei in the evaporation chain for ^{232}Th is a relatively lower peak-to-valley ratio P/V with respect to that of uranium. Another important concern is that the uncertainties due to the extrapolation of the values for the

TABLE II. Calculated and experimental parameters obtained for the mass distribution. The total fission yield Y_F; the position of the two peaks of asymmetric fission, A_L and A_H; the mean mass of the mass distribution (A_S); mean mass of the fissioning nucleus $[(A_f)_{\text{calc}}]$ after evaporation of prescission neutrons from the compound nucleus; mean mass of the fissioning nucleus $[(A_{ff})_{\text{calc}}]$ after evaporation of postscission neutrons from fragments; experimental mean mass of the fissioning nucleus $[(A_f)_{\text{expt}}]$, which includes both type of evaporated neutrons; the values of the peak-to-valley ratios (P/V).

Parameter	^{238}U		^{232}Th	
	$E_{\max} = 50$ MeV	$E_{\max} = 3500$ MeV	$E_{\max} = 50$ MeV	$E_{\max} = 3500$ MeV
$(Y_F)_{\text{expt}}$ (mb/eq.q)	131 ± 20	250 ± 38	40 ± 6	138 ± 21
$(Y_F)_{\text{calc}}$ (mb/eq.q)	149	268.8	39.6	129.6
$(P/V)_{\text{expt}}$	11.4 ± 1.7	2.16 ± 0.40	7.9 ± 1.6	0.84 ± 0.17
$(P/V)_{\text{calc}}$	10.63	6.45	4.80	1.45
$(A_L)_{\text{expt}}$	98.0 ± 1.9	97.0 ± 1.9	91.5 ± 1.8	94.0 ± 1.8
$(A_L)_{\text{calc}}$	98.0	95.0	94.0	95.5
$(A_H)_{\text{expt}}$	137.0 ± 2.7	137.0 ± 2.7	137.5 ± 2.7	134.0 ± 2.6
$(A_H)_{\text{calc}}$	136.0	133.0	134.0	124.5
$(A_S)_{\text{expt}}$	117.5 ± 0.2	117.0 ± 0.2	114.5 ± 0.3	114.0 ± 0.3
$(A_S)_{\text{calc}}$	117.0	114.0	114.0	110.0
$(A_f)_{\text{expt}}$	235.0	234.0	229.0	228.0
$(A_f)_{\text{calc}}$	237.55	235.95	230.61	227.70
$(A_{ff})_{\text{calc}}$	234.0	228.0	228.0	220.0

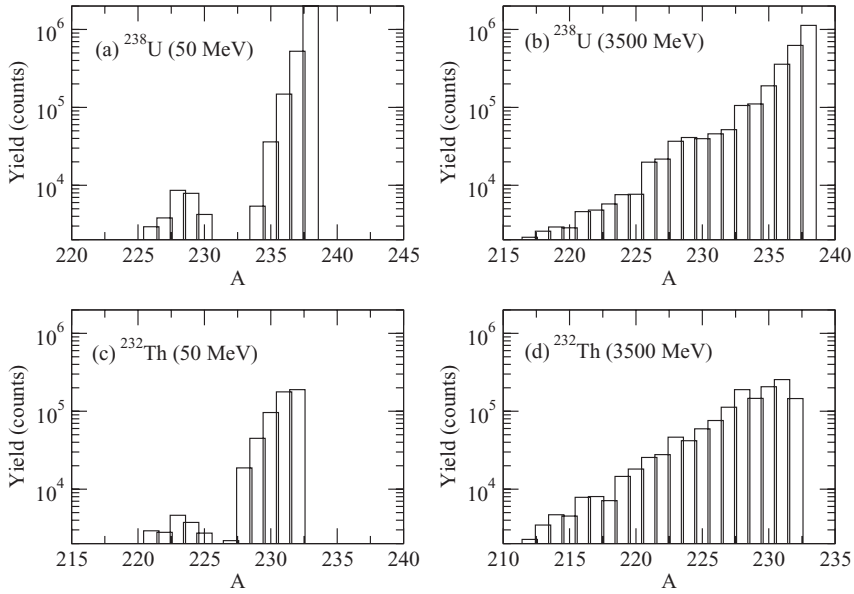

FIG. 6. Initial distribution for fissioning nuclei for [(a) and (b)] ^{238}U and [(c) and (d)] ^{232}Th targets at bremsstrahlung endpoint energies 50 and 3500 MeV, respectively.

parameters in Eq. (1), which is based on the systematic analysis for $A > 220$, are larger in the case of thorium than in the case of uranium. These facts together can explain why the results presented here for ^{238}U are in better agreement with data than for ^{232}Th.

The nature of the interaction of photons and hadrons with nuclei is very different, but the fission process, as mentioned, depends mostly on the excitation of the fissioning nucleus. Thus, to compare data of fission induced by different particles it is useful to use systems with equivalent excitation energy. Our results of fission induced by photons with an endpoint energy of 50 MeV on ^{238}U and ^{232}Th are, thus, compared with fission induced by low-energy protons, neutrons, and alpha particles on the same targets [21,29,41]. The main characteristics of mass distributions such as widths of different fission modes, position parameter D of asymmetric modes, and the average mass number of fragments for the symmetric component, A_S, are in good agreement among these data, giving a clear indication that it is not the incident particle but the structure of the fissioning nucleus and the characteristics of the fragments which determine the mass distribution. A detailed calculation with a statistical model of multimodal fission was performed for intermediate-energy neutrons (200 MeV) by Maslov [30]. It was observed that the largest contribution was obtained for the total fission cross-section events with the emission of 5–7 neutrons on average. This result is in good agreement with our photofission data for 3500 MeV photons (excitation energy around 120 MeV) on both ^{238}U and ^{232}Th targets, where the average number of prefission neutrons is 5. Another comparison that can be made with reactions induced by different probes on ^{238}U and ^{232}Th is the peak-to-valley ratio (P/V) of the mass distribution, which is an indirect way to interpret symmetric and asymmetric mode contributions for fission. The experimental values obtained in the present work together with data obtained for fission induced by photons [42,43], protons [35,36,44], and neutrons [21,30,45] on the same targets are presented in Fig. 7. As can be observed in the figure, there is a general trend for all data of different probes indicating again that it is the excitation energy which is more relevant for the fission process than the type of incident particles.

A systematization of cross sections for symmetric and asymmetric fission in a wide range of nuclei, carried out by Chung *et al*. [35] showed that it is possible to use an empirical expression to estimate the probability of the different fission modes. In order to characterize this factor quantitatively, Chung *et al*. introduced a critical value of the fissility parameter

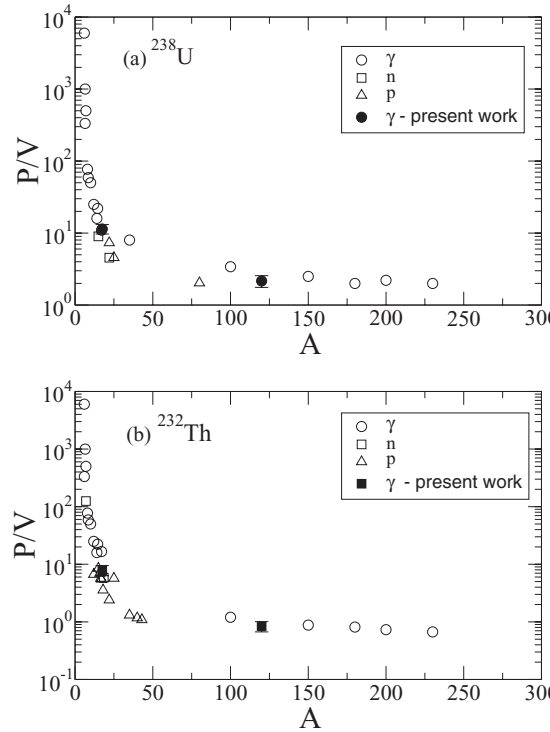

FIG. 7. Peak-to-valley ratio P/V as a function of excitation energy for fission induced by different probes: photon [42,43], protons [35,36,44], and neutrons [21,30,45] on (a) 238U and (b) ^{232}Th targets.

in the form

$$(Z^2/A)_{\text{cr.}} = 35.5 + 0.4(Z - 90), \tag{7}$$

where Z and A are the atomic number and mass of the fissioning nucleus.

Thus, symmetry of the fission-fragment mass distribution is given by the ratio Z^2/A. For nuclei with Z^2/A greater than the critical value, given by Eq. (7), the symmetric fission mode is dominant, while for values below the critical fissility parameter, the fission dynamics led predominantly to asymmetric fragment distributions. For ^{238}U, the parameter $(Z^2/A)_{\text{cr.}}$ is 36.3, and for ^{232}Th it is 35.5. Thus, at low energy (with an average of no more than three evaporated neutrons) for ^{238}U it is natural to expect predominantly asymmetric fission. On the other hand, it is well known that the symmetric component of the fission process increases as the excitation energy of the fissioning nucleus increases. This can be roughly understood as an effect of two factors. The first one is that, with increasing energy, shell effects become less pronounced and, therefore, fission tends to be predominantly symmetric. The other factor is the length of the evaporation chain, which increases as the fissility decreases. Since the evaporation is dominated by neutron emission, longer evaporation chains lead to nuclei in the proton-rich side of the stability valley, and therefore the fissility parameter Z^2/A tends to be above the critical value, resulting in the predominance of symmetric fission.

The fissility of ^{232}Th is lower than that for ^{238}U, and then one can expect that the former nucleus presents a longer evaporation chain. In fact, this can be observed for instance, by the difference of the target nucleus ^{238}U and the mean mass of the fissioning nucleus after evaporation of postscission neutrons, $(A_{ff})_{\text{calc}}$, which for the endpoint photons of 3500 MeV is ten mass units. The same difference is twelve mass units in the case of thorium. This indicates that the evaporation chain is two steps longer in the case of thorium. Also, looking at the peak-to-valley ratio (P/V), it is possible to observe that thorium presents a stronger contribution of symmetric fission when compared with that for uranium.

According to the well-known concept, the fissility is determined as the ratio of the fission yield and the yield of total photon absorption in a nucleus ($D = Y_{\text{tot}}/Y_{\text{abs}}$). In Fig. 8 we plot this fissility D for the ^{238}U and ^{232}Th targets from the present work, together with data for proton-induced fission of ^{241}Am, ^{238}U, and ^{237}Np nuclei [46,47], as a function of the fissility parameter Z^2/A of the fissioning nucleus. We also plot the estimated fissility by the CRISP code for photofission of ^{238}U and ^{232}Th. For the case of ^{238}U one can see that the fission probabilities are about the same, independently of the projectile used to excite the nuclear matter. The calculated fissilities for the thorium target are very close to the experimental values at both energies within the uncertainties. It should be mentioned that the A used to determine the Z^2/A parameter is given by the A_f listed in Table II, which are different for the calculated and experimental values. In the case of the uranium target the calculated values of the

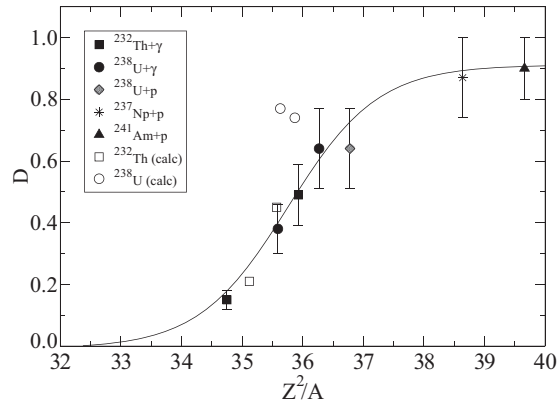

FIG. 8. Fissility D as a function of Z^2/A for $p + ^{237}$Np, p^{238}U, $p + ^{241}$Am [46,47], and $\gamma + ^{238}$U and $\gamma + ^{232}$Th (present work). Calculations by CRISP are open-square and open-circle symbols without error bars. The solid line is to guide the eye through the experimental points.

fissility at both energies overestimate the experimental data, especially for the low-energy photons. This discrepancy may be due to a limitation of the model in taking into account all possible channels of decay of the excited nucleus being considered.

V. CONCLUSION

The present version of the CRISP code, which takes into account different channels of fission, was used to reproduce different aspects of photon-induced fission on actinides. Those calculations allow direct evaluation of the spectrum of fissioning nuclei. The comparison between calculated parameters and data has shown that the calculations describe correctly the main characteristics of charge, such as the most-probable charge for a given fission product mass chain and the width parameter for the photoinduced fission of ^{232}Th and ^{238}U targets at two very different energy regimes (bremsstrahlung photons with endpoint energies of 50 and 3500 MeV). The mass distribution of photofission fragments has been analyzed via the multimodal fission approach. The results presented in this paper show fair agreement between calculation and experiment. The results of the calculations made it possible to determine the fissilities of the fissioning nuclei and compare them with those from other experiments. It was found that CRISP simulations better reproduce data for low-energy photon-induced fissioning systems.

ACKNOWLEDGMENTS

G. Karapetyan is grateful to Fundação de Amparo à Pesquisa do Estado de São Paulo (FAPESP) 2011/00314-0 and to the International Centre for Theoretical Physics (ICTP) under the Associate Grant Scheme. We thank Professor Wayne Seale for reviewing the text.

[1] N. Bianchi *et al.*, Phys. Lett. B **299**, 219 (1993).
[2] J. C. Sanabria *et al.*, Phys. Rev. C **61**, 034604 (2000).
[3] C. Cetina *et al.*, Phys. Rev. Lett. **84**, 5740 (2000).
[4] N. A. Demekhina and G. S. Karapetyan, Phys. At. Nucl. **71**, 27 (2008).
[5] N. A. Demekhina and G. S. Karapetyan, Phys. At. Nucl. **73**, 24 (2010).
[6] A. Deppman, S. B. Duarte, G. Silva *et al.*, J. Phys. G **30**, 1991 (2004).
[7] T. Kodama, S. B. Duarte, K. C. Chung, and R. A. M. S. Nazareth, Phys. Rev. Lett. **49**, 536 (1982).
[8] M. Goncalves, S. dePina, D. A. Lima *et al.*, Phys. Lett. B **406**, 1 (1997).
[9] A. Deppman, O. A. P. Tavares, S. B. Duarte, E. C. de Oliveira, J. D. T. Arruda-Neto, S. R. de Pina, V. P. Likhachev, O. Rodriguez, J. Mesa, and M. Gonçalves, Phys. Rev. Lett. **87**, 182701 (2001).
[10] S. de Pina *et al.*, Phys. Lett. B **434**, 1 (1998).
[11] A. Deppman, O. A. P. Tavares, S. B. Duarte *et al.*, Comp. Phys. Comm. **145**, 385 (2002).
[12] A. Deppman, O. A. P. Tavares, S. B. Duarte, J. D. T. Arruda-Neto, M. Goncalves, V. P. Likhachev, and E. C. deOliveira, Phys. Rev. C **66**, 067601 (2002).
[13] A. Deppman, G. Silva, S. Anefalos, S. B. Duarte, F. García, F. H. Hisamoto, and O. A. P. Tavares, Phys. Rev. C **73**, 064607 (2006).
[14] E. Andrade-II, E. Freitas, O. A. P. Tavares *et al.*, *XXXI Workshop on Nuclear Physics in Brazil* (AIP, New York, 2009) [AIP Conf. Proc. **1139**, 64 (2009)].
[15] S. Anefalos Pereira, A. Deppman, G. Silva, J. R. Maiorino, A. dos Santos, S. B. Duarte, O. A. P. Tavares, and F. Garcia, American Nuclear Society, Nuclear Science and Engineering **159**, 102 (2008).
[16] S. Anefalos, A. Deppman, G. Silva *et al.*, Braz. J. Phys. **35**, 912 (2005).
[17] S. Anefalos, A. Deppman, J. D. T. Arruda-Neto *et al.*, *Int. Conf. on Nuclear Data for Science and Technology* (AIP, New York, 2004) [AIP Conf. Proc. **769**, 1299 (2004)].
[18] S. T. Mongelli, J. R. Maiorino, S. Anefalos *et al.*, Braz. J. Phys. **35**, 894 (2005).
[19] U. Brosa, S. Grossmann, and A. Müller, Phys. Rep. **197**, 167 (1990).
[20] K. Z. Schmidt and B. Jurado, Phys. Procedia **31**, 147 (2012).
[21] W. Younes, J. A. Becker, L. A. Bernstein *et al.*, *Nuclear Physics in the 21st Century: International Nuclear Physics Conference (INPC 2001)* (AIP, New York, 2001) [AIP Conf. Proc. **610**, 673 (2001)].
[22] H. Kudo, M. Maruyama, M. Tanikawa, T. Shinozuka, and M. Fujioka, Phys. Rev. C **57**, 178 (1998).
[23] M. C. Duijvestijn, A. J. Koning, J. P. M. Beijers, A. Ferrari, M. Gastal, J. vanKlinken, and R. W. Ostendorf, Phys. Rev. C **59**, 776 (1999).
[24] C. Wagemans, P. Schillebeeckx, and A. Deruytter, Nucl. Phys. A **502**, 287 (1989).
[25] C. Bockstiegel, S. Steinhauser, K.-H. Schmidt *et al.*, Nucl. Phys. A **802**, 12 (2008).
[26] F.-J. Hambsch *et al.*, Nucl. Phys. A **709**, 85 (2002).
[27] F.-J. Hambsch *et al.*, Nucl. Phys. A **726**, 248 (2003).
[28] H. Weigmann, H. H. Knitter, and F.-J. Hambsch, Nucl. Phys. A **502**, 177 (1989).
[29] T. Ohtsuki, Y. Hamajima, K. Sueki, H. Nakahara, Y. Nagame, N. Shinohara, and H. Ikezoe, Phys. Rev. C **40**, 2144 (1989).
[30] V. M. Maslov, Nucl. Phys. A **717**, 3 (2003).
[31] M. G. Itkis *et al.*, Z. Phys. A **320**, 433 (1985).
[32] I. V. Pokrovsky *et al.*, Phys. Rev. C **62**, 014615 (2000).
[33] C. L. Branquinho and V. J. Robinson, J. Inorg. Nucl. Chem. **39**, 921 (1977).
[34] D. J. Morrissey, W. Loveland, M. de Saint Simon, and G. T. Seaborg, Phys. Rev. C **21**, 1783 (1980).
[35] C. Chung and J. J. Hogan, Phys. Rev. C **25**, 899 (1982).
[36] C. Chung and J. J. Hogan, Phys. Rev. C **24**, 180 (1981).
[37] D. R. Nethaway and B. Mendoza, Phys. Rev. C **6**, 1827 (1972).
[38] J. A. McHugh and M. C. Michel, Phys. Rev. **172**, 1160 (1968).
[39] V. M. Strutinsky, Nucl. Phys. A **122**, 1 (1968).
[40] W. D. Myers and W. J. Swiatecki, Nucl. Phys. **81**, 1 (1966).
[41] A. Matthies, R. Kotte, W. Seidel, F. Stary, and D. Wohlfarth, Z. Phys. A **337**, 439 (1990).
[42] B. Schroder, G. Nydahl, and B. Forkman, Nucl. Phys. A **143**, 449 (1970).
[43] S. A. Karamian, J. Adam, A. G. Belov, J. J. Carroll, Y. V. Norseev, V. I. Stegailov, and P. Chaloun, Phys. Rev. C **62**, 024601 (2000).
[44] H. Kudo, H. Muramatsu, H. Nakahara, K. Miyano, and I. Kohno, Phys. Rev. C **25**, 3011 (1982).
[45] V. M. Gorbachev, Yu. S. Zamiatnin, and A. A. Lbov, *Interaction of Radiation with Heavy Nuclei and Fission* (Atomizdat, Moscow, 1976) (in Russian).
[46] G. S. Karapetyan, A. R. Balabekyan, N. A. Demekhina, and J. Adam, Phys. At. Nucl. **72**, 911 (2009).
[47] A. R. Balabekyan, G. S. Karapetyan, N. A. Demekhina *et al.*, Phys. At. Nucl. **73**, 1814 (2010).